Microchim Acta (2017) 184:3163–3170
DOI 10.1007/s00604-017-2289-x

ORIGINAL PAPER

Amperometric sensing of hydrazine using a magnetic glassy carbon electrode modified with a ternary composite prepared from Prussian blue, Fe_3O_4 nanoparticles, and reduced graphene oxide

Weihua Guo[1,2] · Jianguo Ma[2] · Xiaohong Cao[2] · Xiaolan Tong[2] · Fen Liu[2] · Yunhai Liu[2] · Zhibin Zhang[2] · Shubo Liu[3]

Received: 26 January 2017 / Accepted: 20 April 2017 / Published online: 20 May 2017
© Springer-Verlag Wien 2017

Abstract A magnetic glassy carbon electrode (mGCE) was modified with a ternary composite prepared from Prussian blue (PB), magnetite (Fe_3O_4) nanoparticles, and reduced graphene oxide (rGO) in order to obtain an amperometric sensor for hydrazine. The utilization of Fe_3O_4 facilitates the magnetic immobilization and separation of sensing material, while the use of rGO enhances sensitivity. The surface coverage and the stability of the PB on the modified electrode were considerably improved. The electro-oxidative response to hydrazine was investigated with this modified mGCE using cyclic voltammetry and amperometric. The sensor, typically operated at a voltage of 0.2 V (vs. SCE), displays superior response hydrazine, with a response time of 4 s, a sensitivity of 97.73 μA μM^{-1} cm^{-2} and a 13.7 nM detection limit.

Keywords Magnetite nanoparticles · Reduced graphene oxide · Prussian blue · Hydrazine · Electrocatalysis · Magnetic glassy carbon electrode · Modified electrode

Introduction

As an efficient reducing agent, hydrazine has been widely utilized in many practical applications. Since hydrazine has been considered as a carcinogenic agent which can probably bring damage to liver and brain [1], its determination is practically important for environment protection and health. A number of methods, e.g. spectrophotometry [2], chemiluminescence [3], potentiometry [4] and electrochemical techniques [5], have been reported for the quantitative determination of trace hydrazine. Among these strategies, electrochemical method is worth applying because of its high sensitivity as well as simplicity. So far, numerous chemically modified electrodes, based on redox catalyst such as $Pd–TiO_2$ [6], Vitamin B_{12} [7], *o*-aminophenol [8], benzofuran-CNT/ionic liquids [9] and C@ZnO nanorods [10] have been developed for the detection of hydrazine. Although satisfactory results have been achieved in most attempts, some of them are not eco-friendly when using phenols and benzofuran derivative.

Nowadays, considerable attention has been paid to Prussian blue (PB) modified electrodes in the electrochemical areas for detecting some common molecules such as O_2, hydrogen peroxide and hydrazine [11–13]. However, the high solubility of PB at neutral and basic solutions is the principal handicap for its further application. To enhance the stability and activity of PB-based modified electrodes, numerous materials have been devoted to prepare PB films, such as metal nanoparticles, conducting polymers and carbon materials

Electronic supplementary material The online version of this article (doi:10.1007/s00604-017-2289-x) contains supplementary material, which is available to authorized users.

✉ Yunhai Liu
walton_liu@163.com

✉ Zhibin Zhang
zhang_ecut@hotmail.com

[1] State Key Laboratory Breeding Base of Nuclear Resources and Environment, East China University of Technology, Nanchang, Jiangxi 330013, China

[2] Chemistry, Biological and Materials Sciences Department, East China University of Technology, Nanchang, Jiangxi 330013, China

[3] Jiangxi Province Engineering Research Center of New Energy Technology and Equipment, East China University of Technology, Nanchang, Jiangxi 330013, China

[14–16]. Graphene, a two-dimensional carbon material, has received great attention attributed to its interesting physicochemical properties [17]. Notably, graphene possesses large surface area as well as good chemical stability, which can be used as proper matrix to design PB-based composite nanomaterials. However, graphene tends to aggregate because of the van der Waals interaction, resulting in the loss of its available surface area. Up to now, graphene oxide (GO), the oxygenated derivative of graphene, is utilized as the precursor for preparing graphene-PB composites owing to its good solubility in aqueous [12, 18]. Nevertheless, the electrostatic repulsion between the negative charged PB and reduced form of GO (rGO) is also not conducive to the combination of graphene and PB. Therefore, it is still challenging to develop a new strategy that can effectively improve the electrochemical properties and stability of graphene/PB modified electrode.

Magnetic Fe_3O_4 nanoparticles have been used as promising electrode materials because of their catalysis, magnetic properties, low cost and eco-friendliness [19–21]. However, the major drawback of pristine Fe_3O_4 nanoparticles is that they are more likely to aggregate, resulting in large magnetism loss and poor dispersibility. It has been demonstrated that the combination of Fe_3O_4 nanoparticles with graphene effectively eliminates the self-aggregation possibility of Fe_3O_4 particles and the stacking of individual graphene sheets [19]. The magnetic graphene composites (Fe_3O_4@rGO) provide a valid method for electrode modification and separation problems associated with graphene. Several Fe_3O_4@rGO have been applied in various fields, but only a small part of them have been used for the purposes of electrochemical sensing or biosensing [22].

Study on nanomaterials has increasingly concentrated on combining two or more different constituents in one system owing to their novel and/or enhanced properties that can not be achieved by each constituent [23–26]. Yang et al. have prepared PB/Fe_3O_4/GO composite by an in situ controllable method for the removal of radioactive cesium in water. The combination of PB and Fe_3O_4/GO composite leaded to the improved specific removal efficiency [27]. To the best knowledge of the authors, there is little work undertaken on PB/Fe_3O_4@rGO ternary composite modified electrode applied in hydrazine sensing. Hence, we investigated a sensitive electrochemical sensor by taking the advantage of PB, graphene and magnetic Fe_3O_4 nanoparticles, aiming at providing a reliable and stable method for the determination of hydrazine in aqueous environment. In this paper, PB was synthesized on the surface of Fe_3O_4@rGO by electrochemical deposition approach to prepare a PB/Fe_3O_4@rGO modified electrode which exhibited high stability and excellent sensing performances for electrochemical detection of hydrazine.

Experimental

Reagents and apparatus

Graphite (powder <20 μm) was purchased from Sigma–Aldrich Company, USA (www.sigmaaldrich.com). GO was prepared by the modified Hummers method [28]. All other chemical reagents were utilized without further treatment.

The electrochemical experiments were conducted using a CHI660D analytical system (Shanghai Chenhua Instrument Corp, China, www.chinstruments.com) with a three-electrode system cell. A platinum wire was selected as the counter electrode and a saturated calomel electrode (SCE) was used as reference electrode. PB/Fe_3O_4@rGO modified mGCE was employed as working electrode. The bare mGCE (Φ = 3 mm, magnetic flux density = 0.5 T) was purchased from Gaoss Union Technology Co., Ltd. (Wuhan China, www.gaossunion.com). The diagram of the mGCE was shown in Scheme 1 (part B) and the photos of the actual electrode device were given in Electronic Supporting Material (Fig. S1). Pure nitrogen was bubbled through the solution for 15 min before electrochemical experiments. The electrochemical impedance spectroscopy (EIS) was carried out in 0.5 mM $K_3Fe(CN)_6/K_4Fe(CN)_6$ (1:1) aqueous solution containing 0.1 M KCl with the voltage amplitude of 5 mV in the frequency range from 1 to 10^5 Hz. The morphologies of the samples were recorded by a scanning electron microscope (SEM, Nava NanoSEM 450, www.fei.com). The crystallographic structures of the materials were characterized on a Bruker D8-Advance X-ray diffractometer (XRD, www.bruker.com) with Cu Kα radiation (λ = 1.5418 Å). The Fourier-transform infrared spectra (FTIR) were employed by a Nicolet Nexus-670 spectrometer. Magnetic properties were studied by means of Quantum Design MPMS XL-5 SQUID magnetometer (USA, www.qdusa.com).

Synthesis of Fe_3O_4@rGO composite

Fe_3O_4@rGO was prepared via a hydrothermal method according to the previous report [29]. Briefly, GO (0.33 g) was dispersed in 60 mL ethylene glycol (EG) with the help of an ultrasonic bath. At the same time, 0.72 g $FeCl_3$ was dissolved into another 60 mL EG. The above two solutions were mixed by ultrasonication and then 2.4 g CH_3COONa was added into the solution and stirred vigorously at room temperature for 30 min. Subsequently, the resulting mixture was transferred into a 100 mL Teflon-lined autoclave and heated at 200 °C for 6 h. After cooling to room temperature, the black solid product was isolated from the mixture under magnetic field and washed with ethanol and ultrapure water for several times. Finally, the wet product was dried in vacuum (60 °C). For

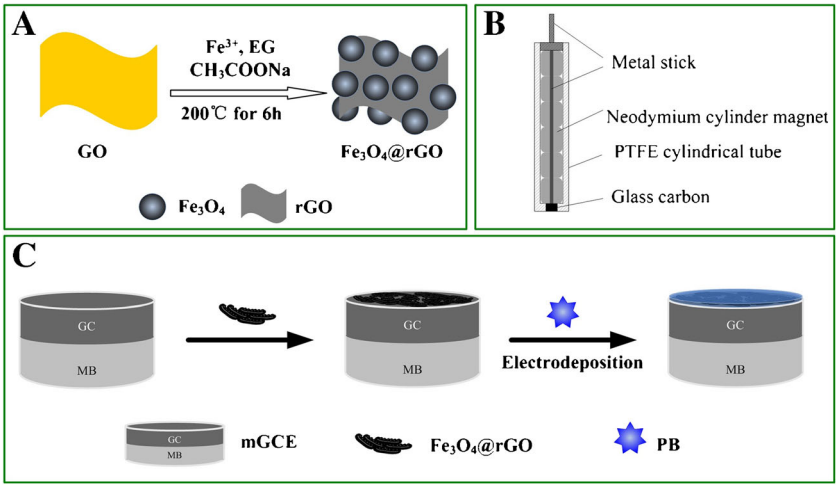

Scheme 1 Schematic illustrations of the preparation process of the Fe_3O_4@rGO composite (**a**), the architecture of mGCE (**b**) and the fabrication process of the PB/Fe_3O_4@rGO/mGCE (**c**)

comparison, the Fe_3O_4 was also synthesized under the same condition without adding GO. The diagram of the preparation process of the Fe_3O_4@rGO composite was illustrated in Scheme 1 (part A).

Preparation of PB/Fe_3O_4@rGO modified electrode

Prior to modification, the mGCE was polished with 0.3 and 0.05 μm α-Al_2O_3 powder, washed successively by ultrasonication in ethanol and water, and then dried in air.

The PB/Fe_3O_4@rGO/mGCE was obtained as follows: 1 mg mL^{-1} Fe_3O_4@rGO suspension was prepared by dispersing a certain amount of Fe_3O_4@rGO in water with ultrasonic agitation for about 30 min. Then, 6 μL of this suspension was dropped onto the cleaned mGCE surface, and dried for 2 h under ambient condition. Later, the Fe_3O_4@rGO/mGCE was immersed in a solution containing 3.0 mM $K_3[Fe(CN)_6]$, 3.0 mM $FeCl_3$, 0.1 M KCl and 0.1 M HCl, and cyclic potential sweep was controlled in the potential range between −0.1 and 1.1 V with a scan rate of 50 mV s^{-1} for 15 circles. After thoroughly washed by distilled water, the PB/Fe_3O_4@rGO/mGCE was activated by applying another 10 cyclic sweeps between −0.1 and 1.1 V in 0.1 M KCl and 0.1 M HCl mixed aqueous solution (Fig. S2). Finally, the PB/Fe_3O_4@rGO/mGCE was dried in air for 1 h to stabilize the formed PB layer. The schematic representation of the fabrication process of the PB/Fe_3O_4@rGO/mGCE was illustrated in Scheme 1 (part C). For comparison, PB/Fe_3O_4/mGCE and PB/mGCE were also fabricated in the same way. Cyclic voltammograms (CVs) were recorded at a scan rate of 50 mV s^{-1}. For the electrochemical detection of hydrazine, different concentrations of hydrazine were added to the stirring N_2-saturated phosphate buffer (0.05 M, pH 6.0, containing 0.1 M KCl) and the generated current was recorded using amperometric technique with an applied potential of 0.2 V.

Results and discussion

Choice of materials

In this approach, Fe_3O_4@rGO composite was used since they can be easily adsorbed on the surface of magnetic glassy carbon electrode (mGCE) under magnetism without any glue, and they can be separated from the surface of the mGCE after the removal of a magnetic field. PB nanoparticles were utilized owing to their excellent reversible redox and catalytic properties. The stability of PB modified electrode is unsatisfactory due to the high solubility of PB in many cases. Herein, PB nanoparticles were synthesized on the surface of Fe_3O_4@rGO through electrochemical deposition approach, in order to improve the stability of PB and at the same time keep its electrochemical activity. The stability of the PB/Fe_3O_4@rGO/mGCE was tested in phosphate buffer using CV for 100 cycles (Fig. 1). The PB/Fe_3O_4@rGO/mGCE shows excellent stability with smaller changes of the peak current after 100 cycles. In contrast, significant decrease of peak current was observed on the PB/mGCE and PB/Fe_3O_4/mGCE after 100 cycles. This result demonstrates that PB/Fe_3O_4@rGO/mGCE possesses better stability than PB/mGCE and PB/Fe_3O_4/mGCE, verifying effective protection of PB with the Fe_3O_4@rGO.

Characterization of Fe_3O_4@rGO composite

The SEM images of Fe_3O_4 and Fe_3O_4@rGO composite are shown in Fig. 2. The Fe_3O_4 particles (Fig. 2a and b) are spherical with an average diameter of approximate 400 nm. The size distribution of Fe_3O_4 is non-uniform because of the agglomerates to large particles [30]. After the combination with GO to form Fe_3O_4@rGO composite (Fig. 2c and d), wrinkled rGO layers and smaller Fe_3O_4 particles with the diameter range from 120 to 270 nm are clearly observed, implying that the Fe_3O_4 microspheres are anchored on the interface of rGO

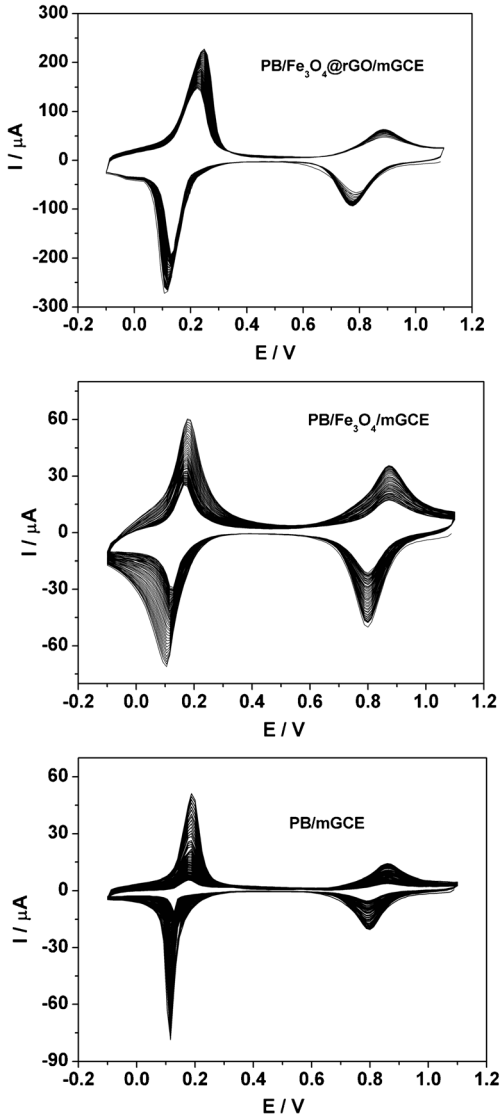

Fig. 1 The CV stability test of PB/Fe_3O_4@rGO/mGCE, PB/Fe_3O_4/mGCE and PB/mGCE for 100 cycles at a scan rate of 50 mV s^{-1} in N_2-saturated phosphate buffer (0.05 M, pH 6.0) containing 0.1 M KCl

layers. The pleat structure of the rGO can prevent the aggregation of Fe_3O_4. Besides, the Fe_3O_4 microspheres can also act as stabilizer to prevent rGO sheets from aggregation [29]. Therefore, the wrinkled flake-like structure can be observed clearly while rGO was decorated with Fe_3O_4 nanoparticles. Such rough structures provide a large effective surface area. This is beneficial for the absorption of electroactive species onto the Fe_3O_4@rGO modified electrode.

The crystalline structures and the chemical bonds of Fe_3O_4@rGO composite were already characterized by using XRD and FTIR, and the results are given in Fig. S3 and Fig. S4. The magnetization curves of Fe_3O_4@rGO composite measured at 300 K are shown in Fig. S5. To obtain an intuitive estimate of the magnetic response of Fe_3O_4@rGO, two photographs of Fe_3O_4@rGO suspension in an applied magnetic field are displayed in inset of Fig. S5. Fe_3O_4@rGO can be easily attracted by placing the mGCE on the side of the container or by immersing the electrode shallowly into Fe_3O_4@rGO suspensions, which is helpful for the modification and separation of Fe_3O_4@rGO on the electrode surface under external magnetic field. The cyclic voltammetric responses and the electron transfer properties of the Fe_3O_4@rGO modified electrode were also investigated and the results are given in Fig. S6 and Fig. S7. The Fe_3O_4@rGO/mGCE presents higher peak current and fast electron transfer kinetics compared to Fe_3O_4/mGCE and bare mGCE, which suggests that the electrical conductivity and electroactive surface area of the composite are increased by the presence of rGO.

Electrochemical characteristics of the PB/Fe_3O_4@rGO/mGCE

To investigate the synergistic effect of the Fe_3O_4@rGO composite, different materials modified electrodes were characterized by cyclic voltammetry. Fig. 3 shows the cyclic voltammograms (CVs) of the PB/Fe_3O_4@rGO, PB/Fe_3O_4 and PB modified mGCE in 0.05 M phosphate buffer (pH 6.0) containing 0.1 M KCl. Two pairs of well-defined redox couples appear on each CVs curve, which are ascribed to the redox processes of PB/Berlin green (BG) and PB/Prussian white (PW), respectively [31]. The two redox processes can be described as follows:

$$\left(\mathrm{PB}\right)\ \mathrm{Fe_4^{III}}\left[\mathrm{Fe^{II}(CN)_6}\right]_3 + 4e^- + 4K^+ \rightarrow (\mathrm{PW})\ \mathrm{K_4Fe_4^{II}}\left[\mathrm{Fe^{II}(CN)_6}\right]_3 \quad (1)$$

$$(\mathrm{PB})\ \mathrm{Fe_4^{III}}\left[\mathrm{Fe^{II}(CN)_6}\right]_3 + 3Cl^- \rightarrow (\mathrm{BG})\ \mathrm{Fe_4^{III}}\left[\mathrm{Fe^{III}(CN)_6}\right]_3 Cl_3 + 3e^- \quad (2)$$

Compared with the PB/mGCE, a significantly increased current is clearly observed for PB/Fe_3O_4/mGCE modified electrodes. This phenomenon may be ascribed that the presence of Fe_3O_4 microspheres increases the surface concentration of PB on the electrode. Obviously, the PB/Fe_3O_4@rGO/mGCE shows the highest peak current in the three modified electrodes, which indicates that the Fe_3O_4@rGO plays an important role to enhance the electroactive surface area as well as the coverage of PB on the electrode surface.

The surface coverage (Γ^*) of PB was evaluated as follow: $\Gamma^* = 4i_pRT/n^2F^2\nu A$, where i_p is the peak current (A), n is the number of electrons transferred per electroactive species, ν is the sweep rate ($V{\cdot}s^{-1}$), A is the geometric area of the working electrode (cm^2). F, R and T have their usual meanings. Taking the second couple of redox peaks as an example, the Γ^* of PB is 1.23×10^{-8} mol cm^{-2} for the PB/Fe_3O_4@rGO/mGCE, which is obviously higher than that obtained from the PB/Fe_3O_4/mGCE (6.11×10^{-9} mol cm^{-2}) and PB/mGCE

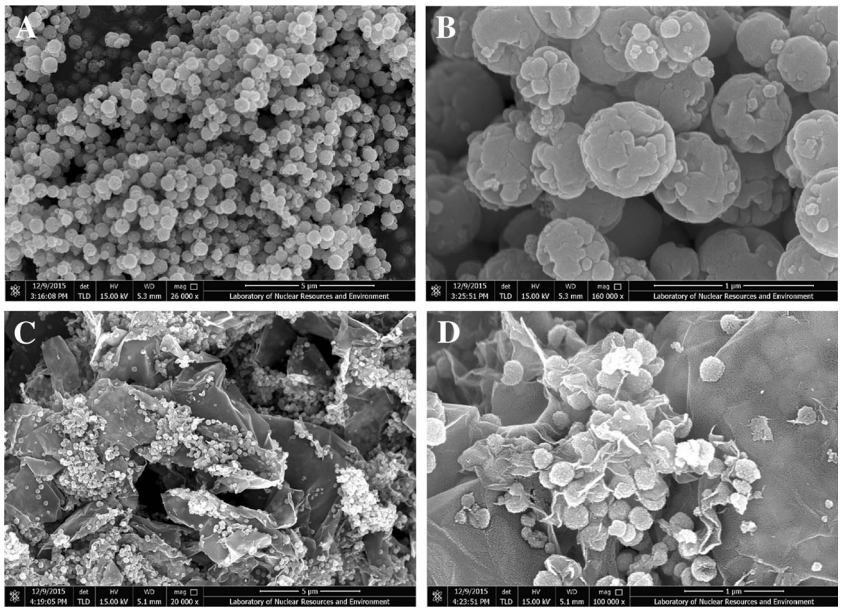

Fig. 2 SEM images of (**a**) Fe_3O_4 nanoparticles and (**b**) Fe_3O_4@rGO composite

(2.81×10^{-9} mol cm^{-2}). Obviously, the existence of Fe_3O_4@rGO significantly enhances the amount of PB. Indeed, the rough surface of Fe_3O_4@rGO can provide the largely exposed surface area to make the increase of PB on the electrode surface.

Optimization of experimental variables

The effects of the magnetic field and film thickness on the electrochemical behavior of the ternary PB/Fe_3O_4@rGO composite modified electrode were studied (See ESM). As exhibited in Fig. S8A and B, the peak current of the PB/Fe_3O_4@rGO prepared with the magnetic field was obviously higher than the other one. In addition, the peak current increases with the increase of cycle number and reaches a maximum at 15 cycles. The influence of scan rates on the voltammetric behavior of PB/Fe_3O_4@rGO/mGCE was also investigated when the scan rate increases from 5 to 600 mV s^{-1} (See Fig. S9). The peak currents are found to be proportional to the scan rate when it is lower than 50 mV s^{-1} (Fig. S9B), indicating the redox process of PB is a surface-controlled process. Fig. S9C shows the relationship of peak current against the square root of the sweep rate over the range from 60 to 600 mV s^{-1}, suggesting that the reaction kinetics change from a surface-controlled process to a diffusion-controlled process.

Amperometric response of the modified electrodes to hydrazine

In this section, the electro-oxidation ability of PB/Fe_3O_4@rGO/mGCE towards hydrazine was studied. To distinguish the contribution of individual modified components and illustrate the potential synergistic effects among them, experiments on the bare mGCE, PB/mGCE and Fe_3O_4@rGO/mGCE were also carried out. Fig. S10 shows

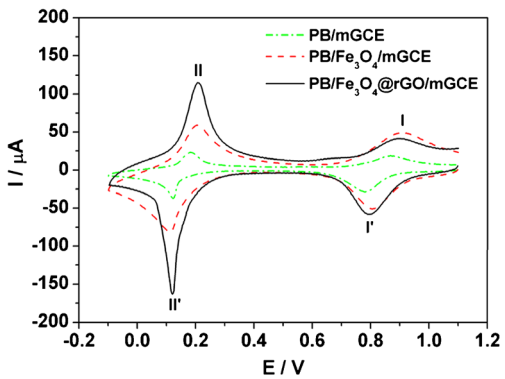

Fig. 3 CVs of PB/Fe_3O_4@rGO, PB/Fe_3O_4 and PB modified mGCE electrodes in 0.05 M phosphate buffer (pH 6.0) containing 0.1 M KCl at 50 mV s^{-1}

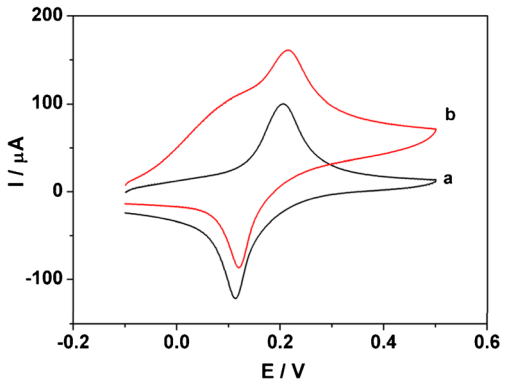

Fig. 4 CVs of PB/Fe_3O_4@rGO/GCE in N_2-saturated phosphate buff (0.05 M, pH 6.0) containing 0.1 M KCl without (**a**) and with (**b**) of 2.5×10^{-5} M hydrazine at a scan rate of 50 mV s^{-1}

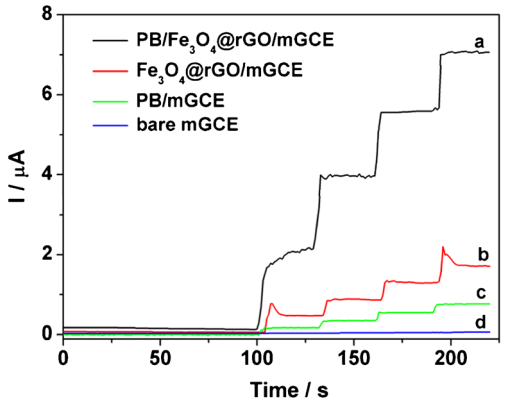

Fig. 5 Amperometric response recorded at PB/Fe_3O_4@rGO/mGCE (**a**), Fe_3O_4@rGO/mGCE (**b**), PB/mGCE (**c**) and bare mGCE (**d**) with the addition of 0.25 μM hydrazine to stirring N_2-saturated PBS. Condition: in 0.05 M phosphate buff (pH 6.0) containing 0.1 M KCl at 0.2 V

the CVs resulting from the bare mGCE, PB/mGCE and Fe_3O_4@rGO/mGCE in 0.05 M phosphate buffer (pH 6.0) containing 0.1 M KCl without (a) and with (b) 2.5×10^{-5} M hydrazine addition. As can be observed, there is a sigmoid like curve, revealing the sluggish electrocatalytic property of bare mGCE for electro-oxidation of hydrazine. CV of Fe_3O_4@rGO/mGCE exhibits an increased oxidation current at potential of +0.35 V which is lower than that at the bare mGCE, indicating good anodic characteristics with fast electrode kinetics. In terms of PB/mGCE, a well-defined oxidation peak at potential of +0.2 V with highly enhanced oxidation current is observed. When the two electrocatalysts are combined together to form PB/Fe_3O_4@rGO modified electrode, an enhancement of anodic peak current, which is the largest among all of the electrodes, can be observed from the CVs presented in Fig. 4. The improved performance is the result of the synergistic effect of Fe_3O_4@rGO and PB nanoparticles. The catalytic mechanism is described as the following reaction process [5, 32]:

$$K_2Fe^{II}[Fe^{II}(CN)_6] \rightarrow KFe^{III}[Fe^{II}(CN)_6] + e^- + K^+ \quad (3)$$

$$4KFe^{III}[Fe^{II}(CN)_6] + N_2H_4 + 4K^+ \rightarrow 4K_2Fe^{II}[Fe^{II}(CN)_6] + N_2\uparrow + 4H^+ \quad (4)$$

Based on the result of Fig. 4, amperometry with the potential of 0.2 V was selected to compare the responses of different electrodes (Fig. 5). It can be seen that both Fe_3O_4@rGO/mGCE (b) and PB/mGCE (c) have electrocatalytic effect towards hydrazine, while the bare mGCE (d) yields negligible response under the same condition. When Fe_3O_4@rGO was applied to immobilize PB, the current of the PB/Fe_3O_4@rGO electrode (a) increases evidently and is greater than the sum of PB and Fe_3O_4@rGO. This enhancement of electrocatalysis is perfectly in agreement with the result obtained by cyclic voltammetry and further confirms the synergistic effect among PB and Fe_3O_4@rGO, which may arise from the good conductor of rGO and 3D structure of Fe_3O_4@rGO. Therefore, a great current response appears for PB/Fe_3O_4@rGO to determine hydrazine. As shown above, PB/Fe_3O_4@rGO/mGCE displays excellent electrocatalytic ability toward the oxidation of hydrazine, and possesses promise for application as electrochemical sensor.

Amperometry is superior to cyclic voltammetry technique for the purpose of sensing because it can provide a fast evaluation on the important characteristics of sensors, such as sensitivity, selectivity and detection limit. Moreover, another advantage of amperometry is that current is measured under an optimal potential where capacitive current is negligible, and

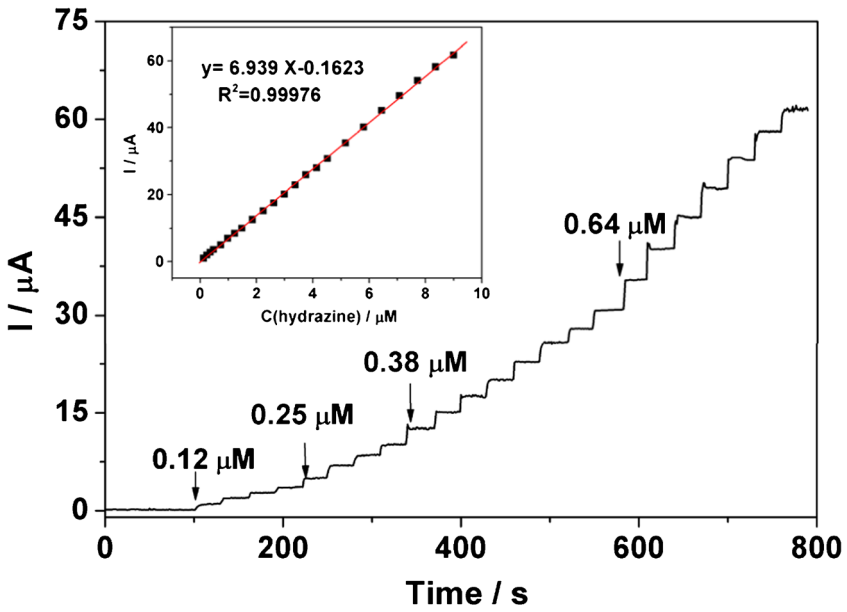

Fig. 6 Amperometric response of PB/Fe_3O_4@rGO/mGCE with successive injection of hydrazine into a stirring N_2-saturated 0.05 M phosphate buffer (pH 6.0) containing 0.1 M KCl at 0.2 V. Inset: calibration curve of hydrazine concentration on the modified electrode

Table 1 Comparative data for hydrazine sensors based on different modified electrodes

Electrode materials	Detection strategy	Potential(V)	LOD[a] (μM)	Sensitivity (μA μM^{-1} cm^{-2})	Reference
PB/SWNTs	Amperometric	0.20	0.5	/	[5]
Pd–TiO_2	chronoamperometric	−0.6	23	0.554	[6]
MWCNT–VB_{12}	Amperometric	0.2	0.7	1.32	[7]
Benzofuran-CNT/ionic liquid composite	DPV[b]	/	0.066	/	[9]
C@ZnO nanorods	Amperometric	0.3	0.1	9.4	[10]
PB-graphene	Amperometric	0.35	7	/	[31]
Tungstophosphate-PAni/silver NCs	I-V method	/	00028	12.5	[34]
PB/Fe_3O_4@rGO	Amperometric	0.20	0.0137	97.732	This work

[a] Limit of detection.

[b] Differential pulse voltammetry

thus the signal-to-noise ratio is increased. Fig. 6 depicts the typical amperometric response of PB/Fe_3O_4@rGO/mGCE examined by successively adding hydrazine into a stirring 0.05 M phosphate buffer (pH 6.0) containing 0.1 M KCl at a working potential of 0.2 V. The electrocatalytic current increases fleetly with the addition of hydrazine solution, and reaches its steady-state value rapidly within 4 s. The obtained response current is linear with the concentration of hydrazine in the range of 0.12 to 9 μM. The linear regression equation is I (μA) = 6.939C (μM) – 0.16231, with the correlation coefficient of 0.99976. Based on the method used in [33], the limit of detection, C_m, is estimated by the equation of $C_m = 3s_{bl}/m$, where s_{bl} stands for the standard deviation of the blank response (μA) and m is the slope of the calibration plot (6.939 μA μM^{-1}). From the above data, the sensitivity and the detection limit of the modified electrode for detecting hydrazine were calculated to be 97.732 μA μM^{-1} cm^{-2} and 0.0137 μM, respectively. Moreover, the performance comparisons of the electrode and other reported results were listed in Table 1. It is exciting to find that the sensor has higher sensitivity and lower limit for hydrazine sensing, demonstrating that the combination of rGO, Fe_3O_4 and PB is more effective in the electroanalysis of hydrazine. Additionally, this modified system is eco-friendly and relatively inexpensive as compared with noble metal materials.

The potential interference of some inorganic ions, which might coexist with hydrazine in environmental system, was investigated with the method of amperometric detection of 1 μM hydrazine. We found that 100-fold of Mg^{2+}, Li^+, NH_4^+, Na^+, K^+, Br^-, NO_2^-, NO_3^-, F^-, SO_4^{2-}, NH_4OH, urea and glucose had no obvious influence on the detection of hydrazine (Fig. S11). The above results indicate excellent selectivity of the PB/Fe_3O_4@rGO modified electrode toward hydrazine.

Conclusions

PB/Fe_3O_4@rGO composite was deposited on mGCE which displayed higher sensitivity and lower detection limit towards hydrazine sensing application by Amperometric method. The sensor exhibits higher-sensitivity (~ 97.732 μA μM^{-1} cm^{-2}) and lower-detection limit (~ 13.7 nM) with good linearity in short response time. These remarkable advantages substantially make PB/Fe_3O_4@rGO modified electrode quite promising for the detection of hydrazine. However, fixed magnetic field strength was employed for the assembly of the ternary composite modified electrode in this paper. Different magnetic field strength should be applied to discuss the structures and electrochemical performances of the modified electrodes, which will be finished in the future work.

Acknowledgements This work is financially supported by the Program for Changjiang Scholars and Innovative Research Team in University (PCSIRT) (No. IRT13054), the National Natural Science Foundation of China (Grant No. 21401022,21461001), the Doctoral Research Fund of East China University of Technology (Grant No. DHBK1007), the Open Project Foundation of the Key Laboratory of Radioactive Geology and Exploration Technology Fundamental Science for National Defense (East China University of Technology) (Grant No. RGET1212) and the Open Project Foundation of State Key Laboratory Breeding Base of Nuclear Resources and Environment (East China University of Technology) (Grant No. NRE1511).

Compliance with ethical standards The author(s) declare that they have no competing interests.

References

1. Garrod S, Bollard ME, Nicholls AW, Connor SC, Connelly J, Nicholson JK, Holmes E (2005) Integrated Metabonomic analysis of the Multiorgan effects of hydrazine toxicity in the rat. Chem Res Toxicol 18:115–122. doi:10.1021/tx0498915
2. Afkhami A, Zarei AR (2004) Simultaneous spectrophotometric determination of hydrazine and phenylhydrazine based on their condensation reactions with different aromatic aldehydes in micellar media using H-point standard addition method. Talanta 62:559–565. doi:10.1016/j.talanta.2003.08.023
3. He ZK, Liu XL, Luo QY, Tang HW, Yu XM, Chen H, Zeng YE (1996) Automatic injection analysis with Chemiluminescence detection: determination of hydrazine. Microchem J 53:356–360. doi:10.1006/mchj.1996.0051

4. Mo JW, Ogorevc B, Zhang XJ, Pihlar B (2000) Cobalt and copper Hexacyanoferrate modified carbon fiber microelectrode as an all-solid potentiometric Microsensor for hydrazine. Electroanalysis 12(1):48–54. doi:10.1002/(SICI)1521-4109(20000101)
5. Wang C, Zhang L, Guo ZH, Xu JG, Wang HY, Shi HW, Zhai KF, Zhuo X (2010) A new Amperometric hydrazine sensor based on Prussian Blue/single-walled carbon nanotube nanocomposites. Electroanalysis 22:1867–1872. doi:10.1002/elan.201000058
6. Yi QF, Niu FJ, Yu WQ (2011) Pd–modified TiO_2 electrode for electrochemical oxidation of hydrazine, formaldehyde and glucose. Thin Solid Films 519(10):3155–3161. doi:10.1016/j.tsf.2010.12.241
7. Umasankar Y, Huang TY, Chen SM (2011) Vitamin B(12) incorporated with multiwalled carbon nanotube composite film for the determination of hydrazine. Anal Biochem 408(2):297–303. doi:10.1016/j.ab.2010.09.037
8. Nassef HM, Radi AE, O'Sullivan CK (2006) Electrocatalytic oxidation of hydrazine at o-aminophenol grafted modified glassy carbon electrode: reusable hydrazine amperometric sensor. J Electroanal Chem 592(2):139–146. doi:10.1016/j.jelechem.2006.05.007
9. Mazloum-Ardakani M, Khoshroo A (2013) An electrochemical study of benzofuran derivative in modified electrode-based CNT/ionic liquids for determining nanomolar concentrations of hydrazine. Electrochim Acta 103:77–84. doi:10.1016/j.electacta.2013.04.062
10. Liu J, Li Y, JiangJ HX (2010) C@ZnO nanorod array based hydrazine electrochemical sensor with improved sensitivity and stability. Dalton Trans 39:8693–8697. doi:10.1039/c0dt00258e
11. Ricci F, Palleschi G (2005) Sensor and biosensor preparation, optimisation and applications of Prussian Blue modified electrodes. Biosens Bioelectron 21(3):389–407. doi:10.1016/j.bios.2004.12.001
12. Bai XY, Chen GH, Shiu K-K (2013) Electrochemical biosensor based on reduced graphene oxide modified electrode with Prussian blue and poly(toluidine blue O) coating. Electrochim Acta 89:454–460. doi:10.1016/j.electacta.2012.11.086
13. Yang JH, Myoung N, Hong HG (2012) Facile and controllable synthesis of Prussian blue on chitosan-functionalized graphene nanosheets for the electrochemical detection of hydrogen peroxide. Electrochim Acta 81:37–43. doi:10.1016/j.electacta.2012.07.038
14. Zou YJ, Sun LX, Xu F (2007) Prussian Blue electrodeposited on MWNTs-PANI hybrid composites for H_2O_2 detection. Talanta 72(2):437–442. doi:10.1016/j.talanta.2006.11.001
15. Zhang J, Li J, Yang F, Zhang BL, Yang XR (2009) Preparation of Prussian blue@Pt nanoparticles/carbon nanotubes composite material for efficient determination of H_2O_2. Sensors Actuators B Chem 143(1):373–380. doi:10.1016/j.snb.2009.08.018
16. Li NB, Park JH, Park K, Kwon SJ, Shin H, Kwak J (2008) Characterization and electrocatalytic properties of Prussian blue electrochemically deposited on nano-au/PAMAM dendrimer-modified gold electrode. Biosens Bioelectron 23(10):1519–1526. doi:10.1016/j.bios.2008.01.009
17. Xu JH, Wang YZ, Hu SH (2017) Nanocomposites of graphene and graphene oxides: synthesis, molecular functionalization and application in electrochemical sensors and biosensors. A review Microchim Acta 184(1):1–44. doi:10.1007/s00604-016-2007-0
18. Li SJ, Du JM, Shi YF, Li WJ, Liu SR (2012) Functionalization of graphene with Prussian blue and its application for amperometric sensing of H_2O_2. J Solid State Electrochem 16(6):2235–2241. doi:10.1007/s10008-012-1653-3
19. He HK, Gao C (2010) Supraparamagnetic, conductive, and processable multifunctional graphene nanosheets coated with high-density Fe_3O_4 nanoparticles. ACS Appl Mater Interfaces 2:3201–3210. doi:10.1021/am100673g
20. Qian J, Wang K, Jin YC, Yang XW, Jiang L, Yan YT, Dong XY, Li HM, Qiu BJ (2014) Polyoxometalate@magnetic graphene as versatile immobilization matrix of $Ru(bpy)_3^{2+}$ for sensitive magneto-controlled electrochemiluminescence sensor and its application in biosensing. Biosens Bioelectron 57:149–156. doi:10.1016/j.bios.2014.02.005
21. Su J, Cao MH, Ren L, Hu CW (2011) Fe_3O_4–graphene nanocomposites with improved lithium storage and magnetism properties. J Phys Chem C 115(30):14469–14477. doi:10.1021/jp201666s
22. Teymourian H, Salimi A, Khezrian S (2013) Fe_3O_4 magnetic nanoparticles/reduced graphene oxide nanosheets as a novel electrochemical and bioeletrochemical sensing platform. Biosens Bioelectron 49:1–8. doi:10.1016/j.bios.2013.04.034
23. Leveneur J, Waterhouse GIN, Kennedy J, Metson JB, Mitchell DRG (2011) Nucleation and growth of Fe nanoparticles in SiO2: a TEM, XPS, and Fe L-edge XANES investigation. J Phys Chem C 115(43):20978–20985. doi:10.1021/jp206357c
24. Fang F, Kennedy J, Futter J, Hopf T, Markwitz A, Manikandan E, Henshaw G (2011) Size-controlled synthesis and gas sensing application of tungsten oxide nanostructures produced by arc discharge. Nanotechnology 22(33):335702. doi:10.1088/0957-4484/22/33/335702
25. Kaviyarasu K, Manikandan E, Kennedy J, Jayachandran M, Maaza M (2016) Rice husks as a sustainable source of high quality nanostructured silica for high performance li-ion battery requital by sol-gel method – a review. Adv Mater Lett 7(9):684–696. doi:10.5185/amlett.2016.6192
26. Kaviyarasu K, Manikandan E, Kennedy J, Maaza M (2015) A comparative study on the morphological features of highly ordered MgO:AgO nanocube arrays prepared via a hydrothermal method. RSC Adv 5(100):82421–82428. doi:10.1039/C5RA15132E
27. Yang HJ, Sun L, Zhai JL, Li HY, Zhao Y, Yu HW (2014) In situ controllable synthesis of magnetic Prussian blue/graphene oxide nanocomposites for removal of radioactive cesium in water. J Mater Chem A 2:326–332. doi:10.1039/C3TA13548A
28. Marcano DC, Kosynkin DV, Berlin JM, Sinitskii A, Sun ZZ, Slesarev A, Alemany LB, Lu W, Tour JM (2010) Improved synthesis of graphene oxide. ACS Nano 4:4806–4814. doi:10.1021/nn1006368
29. Ai L, Zhang C, Chen Z (2011) Removal of methylene blue from aqueous solution by a solvothermal-synthesized graphene/magnetite composite. J Hazard Mater 192(3):1515–1524. doi:10.1016/j.jhazmat.2011.06.068
30. Sun YF, Chen WK, Li WJ, Jiang TJ, Liu JH, Liu ZG (2014) Selective detection toward Cd^{2+} using Fe_3O_4/RGO nanoparticle modified glassy carbon electrode. J Electroanal Chem 714-715:97–102. doi:10.1016/j.jelechem.2013.12.030
31. Jiang Y, Zhang X, Shan C, Hua S, Zhang Q, Bai X, Dan L, Niu L (2011) Functionalization of graphene with electrodeposited Prussian blue towards amperometric sensing application. Talanta 85(1):76–81. doi:10.1016/j.talanta.2011.03.028
32. Zhao J, Liu J, Tricard S, Wang L, Liang Y, Cao L, Fang J, Shen W (2015) Amperometric detection of hydrazine utilizing synergistic action of prussian blue@silver nanoparticles/graphite felt modified electrode. Electrochim Acta 171:121–127. doi:10.1016/j.electacta.2015.05.027
33. Skoog DA, Holler FJ, Nieman TA (1998) Principles of instrumental analysis, fifth edn. Harcourt Brace, Philadelphia
34. Rahman MM, Khan A, Marwani HM, Asiri AM (2016) Hydrazine sensor based on silver nanoparticle-decorated polyaniline tungstophosphate nanocomposite for use in environmental remediation. Microchim Acta 183(5):1787–1796. doi:10.1007/s00604-016-1809-4